Adaptive finite element simulation of fretting wear and fatigue in a taper junction of modular hip prosthesis

Ali Cherif Messellek, Mohand Ould Ouali, Abdelwaheb Amrouche

Adaptive finite element simulation of fretting wear and fatigue in a taper junction of modular hip prosthesis

Ali Cherif Messellek [a], Mohand Ould Ouali [b], Abdelwaheb Amrouche [c,*]

[a] Laboratoire Conception des Systèmes Mécaniques (LCSM), École Militaire Polytechnique, BP 17, 16111, Alger, Algérie

[b] Laboratory Elaboration and Characterization of Materials and Modelling (LEC2M), Mouloud MAMMERI University of Tizi-Ouzou, BP 17RP, 15000, Tizi Ouzou, Algeria

[c] Univ. Artois, Univ. Lille, IMT, Yncrea, Laboratoire Génie Civil et géo-Environnement (LGCgE, EA 4515), Technoparc Futura, 62400 Béthune, France

* Corresponding author: Professor Abdelwaheb Amrouche; abdelwaheb.amrouche@univ-artois.fr

Abstract

Modular taper junctions are commonly used in total hip arthroplasty to offer a wide range of intraoperative choices to surgeons. The damage at the taper surfaces can lead to the implant failure either by material removal (wear) or by cracks nucleation (fatigue). This paper presents a methodology based on the finite element approach to study both fretting wear and fatigue, taking into account their interaction in the modular taper. The modified Archard's law was employed to compute wear depth and the corresponding volume loss while the fatigue life was predicted using two critical plane fatigue parameters (Smith-Watson-Topper and Fatemi-Socie). An adaptive meshing technique was implemented to take into account the geometry changes and the material removal effect on fatigue life. The methodology developed was discussed and validated against available experimental data from the literature. In this case considered, a transition from a partial slip regime to a large slip one, which is mainly controlled by the contact slip amplitude, was found to reduce the fatigue life and a critical slip value was identified. This provides an efficient tool for an in-depth understanding of fretting in taper junctions and for future design.

Keywords: fretting; wear; fatigue; crack; total hip prosthesis; taper junction.

1. Introduction

Total hip replacement (THR) is recognized as one of the most successful surgical solutions performed to restore hip biomechanics and resume the patient normal life. According to its morphology, the surgeon chooses the appropriate prosthesis to replace the damaged hip joint. Prostheses with modular femoral neck offer a wide range of intraoperative choices to surgeons by varying many parameters such as neck offset, leg length and collum-caput-diaphysis (CCD) angle. Furthermore, it can be possible to combine different materials and obtain better biocompatibility [1]. Modular total hip prosthesis (THP) is constituted of a spherical femoral head connected to the femoral stem using a conical taper junction. Despite its various benefits, the additional contact interface in head-neck or neck-stem junctions can lead to the potential for failures and high rate of surgery revision [2].

In the literature, numerous retrospective studies and case reports were conducted to identify the causes of failure associated with modular implants. Fokter et al. [3] reviewed a large number of reports published in the period 2010-2016 on the failure of modular hip prosthesis. The study was based on data provided by the Food and Drug Administration (FDA, USA), the Australian arthroplasty registry (AOANJRR) and the European arthroplasty registries. They concluded that the main forms of failure were fretting, subsurface micro-cracks, corrosion and overload of the neck. In a similar study, Osman et al. [4] revealed that fretting and corrosion within the metal on metal (MoM) taper junctions contribute to the generation of small metal wear debris. The excessive level of metal ions causes the formation of adverse local tissue reaction and lymphocytic inflammatory cells leading to severe complications. Recently, many authors reported the fatigue fracture and failure of the modular component as a potentially serious failure mode but under-documented in the literature. Goldstein et al. [5] reported the failure of Large-Diameter Metal-on-Metal THP of a 54-years-old man after ten years of use. The femoral head was dissociated after the breakage of the femoral neck due to a fatigue injury. Ullmark et al. [6] identified a one-year mortality rate of 24% in elderly patients after neck fracture. Likewise, Williams et al. [7] demonstrated nucleation of subsurface fatigue crack on the anterolateral side of the implant's neck of a failed Ti6Al4V Profemur Z implant. High fretting marks and corrosion were observed at this region of the neck than on other

surfaces. These retrospective studies, in their majority, revealed that both of fretting wear and fatigue are the potential failure cause of modular hip prosthesis.

In-vitro studies were undertaken to analyze fretting mechanisms in taper junctions using representative test devices as in [8–11]. However, in-vitro tests remain very expensive, limited and require a long lead time. This is due to the long exposure of the implant to cyclic loading and the difficulty to capture the variation of mechanical quantities over time. In parallel, computational simulations were developed to further investigate different aspects of fretting in modular junctions of hip implants. English et al. [12; 13] developed a methodology based on a 3D-FE model and energy wear approach to study the effect of assembly load on fretting wear in taper junctions. Similarly, the effect of angular mismatch on the fretting wear process was investigated by Fallahnezhad et al.[14]. The Archard wear equation was implemented for an adaptive 2D-FE modeling. The developed model was combined with existing empirical electrochemical equations to simulate the process of fretting corrosion within CoCr/CoCr interfaces and the induced material loss [15]. Ashkanfar et al. [16] also studied the effect of varying taper mismatch using an energy-based wear approach. However, most of the studies available in the literature investigated only the fretting wear behavior without any consideration of interaction with fatigue, despite its major effect clinically and experimentally proven.

Interaction between fretting wear and fatigue was well studied and documented in other engineering applications [17–21]. In contrast, few studies considered this aspect in the case of modular hip junctions. Baxmann et al. [22] conducted an experimental investigation using a device similar to taper coupling used in the hip prosthesis. Fretting wear was observed in the case of high micromotions combined with low contact pressures. Fretting fatigue was found for low micromotions and high contact pressures. Zhang et al. [23; 24] developed a 2D axisymmetric model of a 12/14 modular neck taper to study the wear effect on the contact interface and the consequent fatigue life. The energy-based approach and the Smith–Watson–Topper (SWT) fatigue parameter were employed to compute wear and fatigue life, respectively. The authors found low values of wear depth and fatigue life exceeding one hundred million cycles. This was due to the use of a 2D axisymmetric model and the simplification of the applied load so that only the axial load was considered. According to Bergmann et al. [25], the loads applied on the hip implant are multidirectional and non-symmetric. The simplification of these loads to be applicable for simulators and numerical analyses should not be at the expense of realistic in vivo loads.

The main purpose of this study is to improve the comprehension of mechanical behavior within a modular taper junction subjected to cyclic loading. This investigation is pertinent in that it considers the interaction between fretting wear and multiaxial fatigue mechanisms and their effects on the service life of a modular THP. The methodology proposed here is a three-dimensional finite element analysis based on (i) A modified version of the Archard equation to quantify wear depth and volume loss evolving, (ii) Two multiaxial fatigue criteria coupled with a linear damage accumulation law implemented to predict the lifetime, and (iii) An adaptive meshing framework introduced to capture the effect of geometry changes and investigate the interaction between wear and fatigue. The wear depth, rate, scar and fatigue life are found to be comparable with those available in the literature. The developed methodology could be employed to identify the fretting regime and the slip amplitude leading to the failure so that to avoid them in the design of new modular hip prostheses.

2. Methods

2.1. Wear modeling and implementation

The simulation of fretting wear in contact interfaces is based on local modeling of wear. For this purpose, the modified version of Archard equation (see McColl et al. [26]) is herein employed. For a given point in the contact area, the local wear depth is described by:

$$\dot{h} = k_l p \dot{s} \tag{1}$$

where h, p and s are the local wear depth, the contact pressure and the relative contact slip, respectively. k_l represents the local wear coefficient, which is assumed to be equal to the volumetric wear coefficient k as justified in Refs. [26] and [27].

The wear process is applied to the defined contact nodes of the FE model described in section 2.4. Hence, for each contact node n at the m^{th} increment, the incremental wear depth is provided by:

$$\Delta h_n^m = k p_n^m \Delta s_n^m \tag{2}$$

The integration of the incremental wear depth is done on small increments of time. For a high number of loading cycles, the full simulation would require a very high computational time. To overcome this, the cycle jump

technique is employed and the integration is done on a block of ΔN fretting cycles. The cycle jump factor ΔN is determined in such a way that the contact variation remains constant over the ΔN cycles. Therefore, the wear depth is calculated as follows:

$$\Delta h_n^m = k \Delta N p_n^m \Delta s_n^m \tag{3}$$

$$h_n = \sum_{i=1}^{N_{total}/\Delta N} \sum_{m=1}^{M} \Delta h_n^m \tag{4}$$

h_n being the accumulated wear depth for a given contact node n; N_{total} is the applied load cycles, and M is the maximum increment number within one load cycle.

The implementation of the Archard modified wear equation is achieved using the user-defined subroutine UMESHMOTION provided in ABAQUS software package. This subroutine gives the contact results and computes the incremental wear depth for each node inside the adaptive domain. Then, the material removal is done after the end of each converged increment. This can be carried out through the adaptive meshing framework of ABAQUS, which is based on the Arbitrary Lagrangian-Eulerian (ALE) algorithm. The ALE meshing is achieved in two steps in a Eulerian analysis. Firstly, the surface nodes within the adaptive domain move in the local normal direction according to the constraints defined in UMESHMOTION and a mesh sweeping is done after. Secondly, the material quantities are re-mapped from the old mesh to the new swept mesh by solving the advection equations using the Lax-Wendroff method [28]. **Figure 1** depicts an exaggerated illustration of the geometry updated after wear.

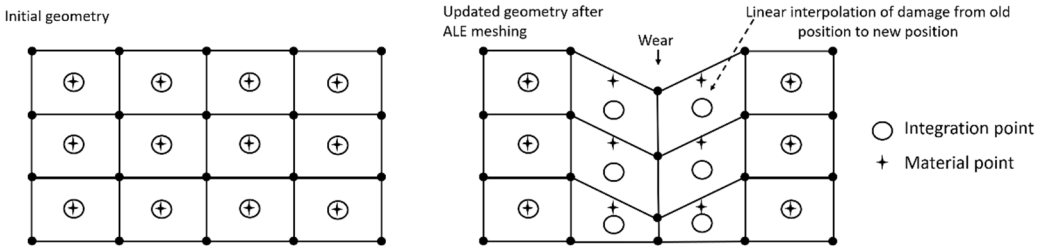

Figure 1: Schematic illustration of ALE meshing and damage interpolation

2.2. Fatigue modeling and implementation

Cyclic loadings applied on hip prosthesis are considered as multiaxial and non-proportional complex stresses. They involve tensile, compressive and shear stresses leading to different crack initiation modes. For this reason, two critical plane multiaxial fatigue parameters are used in this study, namely the Smith-Watson-Topper (SWT) and the Fatemi-Socie (FS). The critical plane criteria have been satisfactorily used by many researchers for the prediction of crack nucleation life under such fretting problems [19]. In the previous work [29], with another contact configuration, we have compared the prediction with different fatigue parameters. The SWT fatigue parameter is based on the combination of the Coffin-Manson's rule (plastic strain component) and the Basquin's rule (elastic strain component). It is given by the following relationship [30]:

$$SWT = \sigma_{\max} \frac{\Delta \varepsilon}{2} = \frac{(\sigma'_f)^2}{E} (2N_f)^{2b} + \sigma'_f \varepsilon'_f (2N_f)^{b+c} \tag{5}$$

where $\sigma_{\max}$ is the maximum normal stress on the critical plane and $\Delta\varepsilon$ is the normal strain amplitude in the same plane. σ'_f and b are the fatigue strength coefficient and exponent, while ε'_f and c are the fatigue ductility coefficient and exponent, E is Young's modulus and N_f is the number of cycles to crack initiation. For cracks that initiate on planes of high shear strain, the FS fatigue parameter is applied and it is done via **Eq 6** [30].

$$FS = \frac{\Delta\gamma}{2}\left(1 + \alpha \frac{\sigma_{\max}}{\sigma_y}\right) = \frac{\tau'_f}{G}(2N_f)^b + \gamma'_f (2N_f)^c \tag{6}$$

where $\Delta\gamma$ is the amplitude of shear strain in the critical plane, σ_y is the yield strength, and α is a constant. G is the shear modulus, and τ'_f and γ'_f are constants.

In this work, the implementation of this approach is performed according to the methodology described in [31] for both parameters. This methodology is based on the 3D transformation of the stress/strain of each element

integration point and at each increment of the simulated loading cycle. The transformation is done on two circles of 180° with a step of 5° which results in 1296 planes for each element. This procedure is repeated for each element at each time increment to find the maximum value of SWT and FS of the entire fretting cycle. The corresponding numbers of cycles to failure can be numerically determined via **Eqs 5** and **6**.

2.3. Combined wear-fatigue model

The material removal results in a change of the contact geometry, thus affecting the stress-strain distribution near the contact surface from cycle to cycle. To capture this evolution, the fatigue damage corresponding to each $_{\Delta N}$ cycle is calculated for each element. The linear accumulation rule of Miner-Palmgren is used for accumulating the fatigue damage, as follows [32]:

$$D = \sum_{i=1}^{N_{total}/\Delta N} \frac{\Delta N}{N_{f_i}} \tag{7}$$

where N_{f_i} is the corresponding number of cycles to failure, previously predicted using **Eqs 5** and **6**. When the total accumulated damage $_{D}$ reaches a critical value, the crack initiation is assumed to occurred at this location.

As up mentioned, the accumulated damage is computed based on the assessment of stress-strain in each element integration point. However, as a consequence of mesh updating due to the material removal, the damage accumulation is going to be done in two different integration points from one fretting cycle to another. This gives an incorrect result of damage, since the integration points are no longer linked to the same material points. Thereby, the difference between a material point and a mesh integration point has to be considered. This problem has often been overcome by the use of the material point mesh (MPM) method, initially developed by Madge et al. [33]. For this method, these authors proposed to define fixed coordinates of MPM nodes independently of the FE mesh. Then, the damage is linearly interpolated back according to the MPM for the accumulation while excluding the removed material nodes, as illustrated in **Fig 1**.

2.4. Finite element model description

The developed 3D model consists of a femoral stem that ends with a Type 1 taper (4°) and a matching taper adaptor (**Fig 2a**). The stem is potted in the cement and the assembly of the different parts is done according to ISO 7206-6:2013. The stem and adaptor are both assigned with properties corresponding to titanium alloy Ti6Al4V, while the cement is assigned with properties of polymethyl methacrylate (PMMA).

The meshing is carried out in such a way to further refine the contact zones represented by the adaptive domain, while coarse meshes are used in regions away from the contact zones. All models are meshed with the 8-nodes linear brick, reduced integration elements (C3D8R). The mesh size of contact elements and the cycle jump factor (ΔN) are determined following a convergence study, which will be discussed in subsection 3.1.

A tied contact is defined between the cement and the femoral stem to ensure a full fixation. The master-slave algorithm using the finite sliding contact formulation is employed to define the contact interaction between the taper adaptor (master surface) and the taper (slave surface). In addition, the isotropic penalty formulation is used to obtain a good contact convergence, and according to experimental tests carried out on specimens of implant taper made of Ti6Al4V [34], a friction coefficient of 0.29 was applied. The Archard wear coefficient $k$of Ti6Al4V was set to 2.75 mm^3/N.mm based on the results reported by Madge et al.[33]. Besides, the elastic behavior properties and fatigue parameters corresponding to Ti6Al4V were taken from [30].

To assemble the taper adaptor on the taper, a 4 kN load is applied [35] while the exterior cement potting nodes are fully fixed in translation. Then, a sinusoidal load equivalent to walking forces is applied with a maximum of 4 kN and a minimum of 400 N. A kinematic coupling was created between the outside surface of the adaptor and the reference node of the force vector. The applied load, boundary conditions and constraints are illustrated in **Fig 2a**. The load was oriented according to the standard ISO 7206-6:2013, which requires an angle of 9° in the sagittal plane and 10° in the coronal plane (**Fig 2b**). The CCD angle was fixed at 135°. The global implementation steps of the developed methodology are gathered in **Fig 3**.

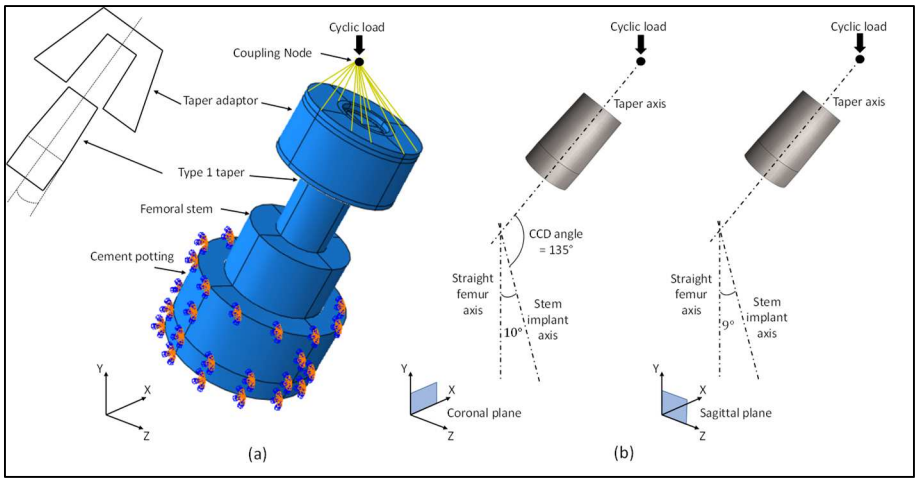

Figure 2: Illustration of (a) 3D FE model and boundary conditions (b) 3D orientations

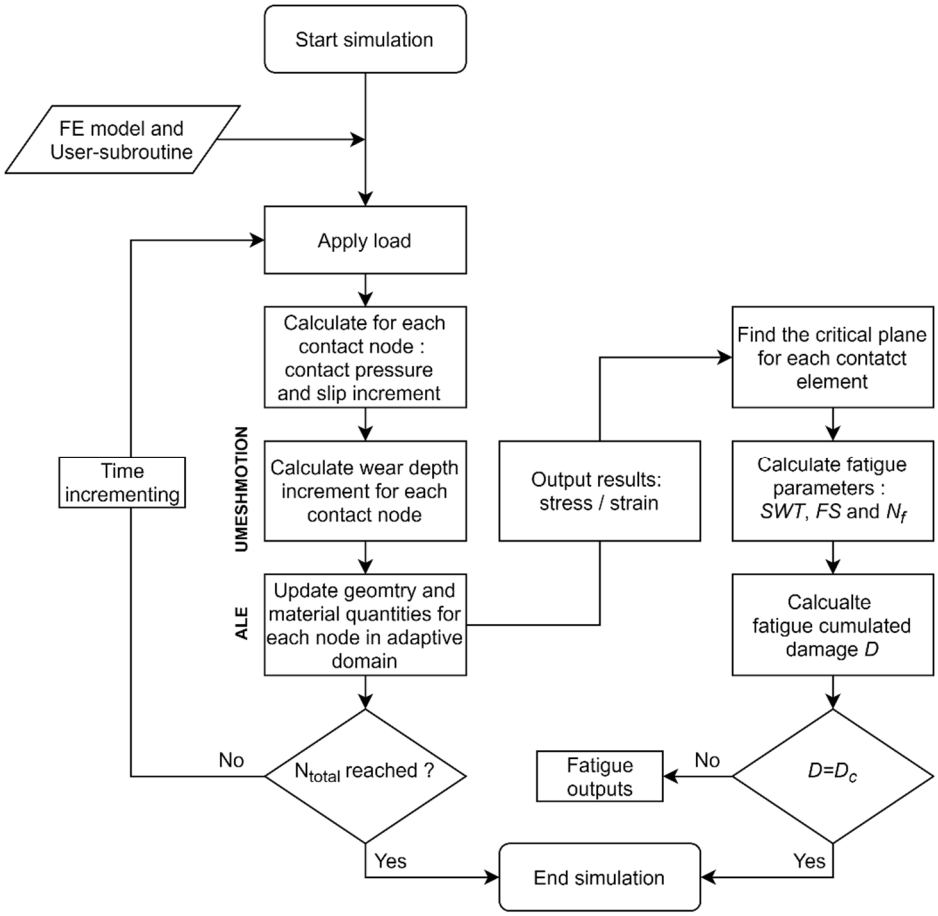

Figure 3: Flowchart of the main steps of the developed methodology

3. Results

3.1. Computational time optimization

The developed methodology is based on a 3D- FE simulation, which requires a high computational time. The high number of cyclic loadings analyzed in this study increases drastically the total computing time for the full simulation. The mesh size of the contact zone and the cycle jump factor (ΔN) were identified in similar studies as the most influencing parameters on computational time [36; 37]. In this section, the optimization of the two main parameters is performed to reduce the computational time. To obtain more correct convergence results, two wear scar profiles are considered in this analysis. The first is the circular profile of the bottom contact edge, while the second is the median profile towards the proximal contact edge of the taper (**Fig 4**). In addition, the

relative error between two subsequent simulation results is calculated to analyze the convergence using **Eq 8** (see [38]) :

$$e_{rel} = \left| \frac{\phi_{\max}^{i+1} - \phi_{\max}^{i}}{\phi_{\max}^{i+1}} \right| \tag{8}$$

where $\phi_{\max}^{i}$ is the maximum variable output in the ith simulation and $\phi_{\max}^{i+1}$ correspond to the (i+1)th simulation.

It should be pointed that for all simulations of the convergence study, the total number of cyclic loading is fixed at 2 million. This was performed based on a computational time estimation.

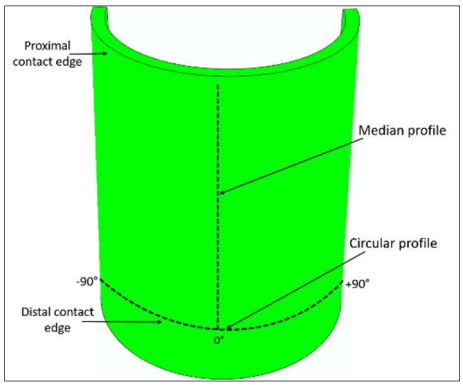

Figure 4: Profiles and contact edges location on the taper

3.1.1. Effect of mesh size

The mesh size in the contact zone is the most important parameter affecting the total computational time of the simulation. In this optimization analysis, the cycle jump factor is fixed to 10,000 and the mesh size range is 0.05 to 0.5 mm. **Figure 5** shows the mesh size effect on the dimension and the shape of the wear scar profile. For the coarse mesh, a relatively small wear scar is produced, either on the circular or median profile. It can be seen that, as the mesh size decreases, the wear scar profile widens in both profiles and becomes more similar and uniform in cases of a refined mesh. The relative error in wear depth decreases and reaches a maximum of 3.5% between cases
of 0.25 and 0.1 mm mesh size. Based on these results, a mesh size less than 0.25 mm is sufficient for the convergence of a fretting wear simulation. Nevertheless, this mesh size is found to give a poor discretization for computing of fatigue parameters SWT and FS. **Figure 6** shows an obvious difference in shape and amplitude of both fatigue parameters according to the mesh size. However, the use of a more refined mesh (0.1 and 0.05 mm) has stabilized the convergence and reduced the relative error to 2% for SWT and 2.3% for FS computing. On the other hand, the total computational time is found to be reduced four times using a mesh size of 0.1 mm compared to a mesh of 0.05 mm. Based on this analysis; a 0.1 mm mesh size is selected.

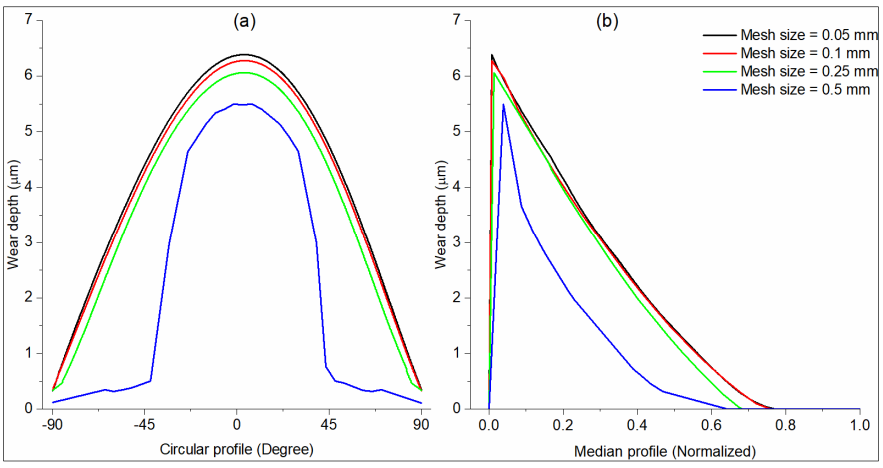

Figure 5. Effect of mesh size on the wear depth predicted along (a) circular profile and (b) median profile

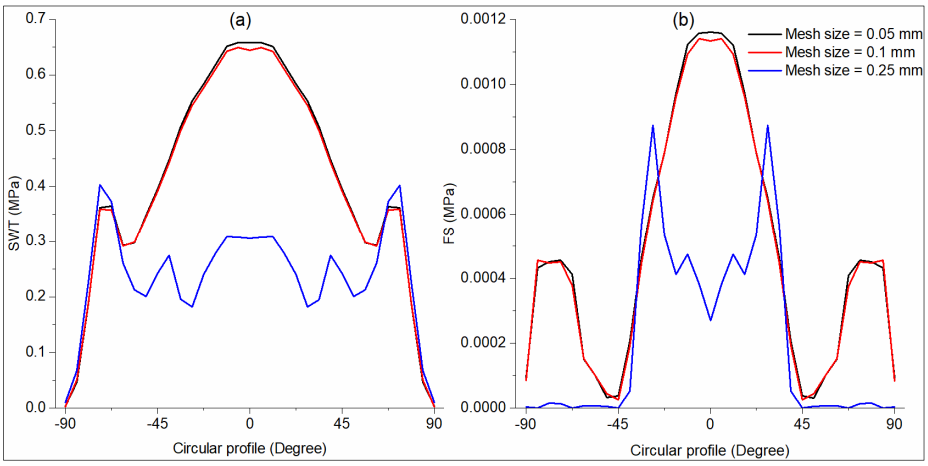

Figure 6. Effect of mesh size on: (a) SWT parameter (b) FS parameter

3.1.2. Effect of cycle jump factor

The second parameter studied here is the cyclic jump factor which is based on the determination of the maximum wear increment using **Eq 3**. According to McColl et al. [26], the use of a larger value of ΔN reduces the computational time but can significantly affect the stability of the results. Recall that, for this analysis, the mesh size was set to 0.1 mm and the range of cycle jump factor was 5,000 to 50,000 cycles.

Figure 7 reveals the strong influence of ΔN on both profiles of the wear scar and the corresponding predicted wear depth. When the factor is too large (ΔN = 50,000), the wear scar is narrower and deeper with additional peaks at the circular profile. While, for a small value of ΔN (less than 20,000), the cycle jump factor has practically no effect, either on the wear scar shape or on the predicted wear depth. A relative error in depth less than 2% was obtained between cases of ΔN =10,000 and ΔN =5,000 cycles. In addition, the computational time required for ΔN =10,000 is half as long as for ΔN =5,000. Thereby, a cyclic jump factor of 10,000 is retained.

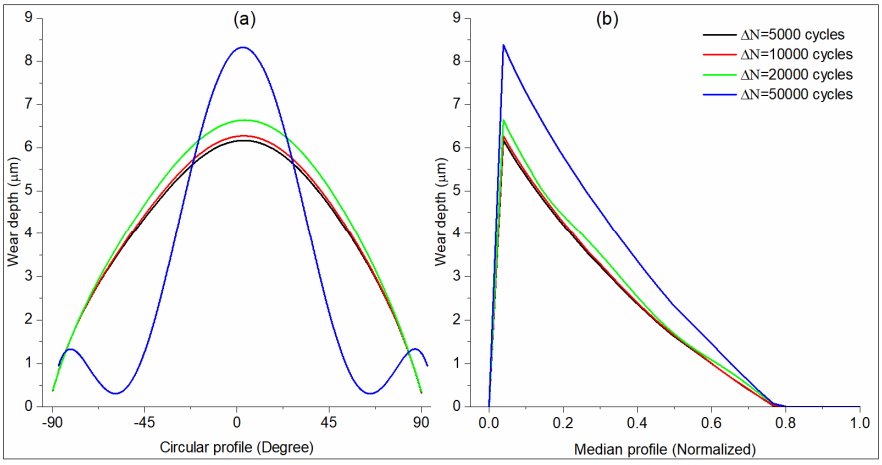

Figure 7. Cycle jump factor's effect on the wear depth predicted along (a) circular profile and (b) median profile

3.2. Methodology validation

Because of the complexity and the high cost of experimental tests on modular hip prostheses, very few experiments were reported in the literature. To compare the results and validate the proposed methodology, the FE model described in section 2.4 was developed so that it is similar to the experimental setup used by Bitter et al. [8], [35]. These authors carried out three accelerated fretting tests of 10 million sinusoidal cyclic loading on Type 1 Zimmer Biomet taper. Both of FE model and experimental test were set up according to the ISO 7206-6:2013 standard, which specifies the test conditions for investigating of THP neck region.

This sub-section presents a comparison between the results of the computational methodology developed in this study, and the experimental results available in the literature [8], [35]. **Figure 8a** shows a noticeable similarity between the FE simulated wear scar and that produced experimentally. The wear marks are mainly observed in the middle of the contact edge of the inferior side with a gradual decrease towards the median region of the taper. Furthermore, conservative prediction of wear depth is obtained by the FE-simulation compared to the measured experimental values, as presented in **Fig 8b**. The experimentally measured wear depth is found to be 30.5±17.3 µm while the maximum FE-predicted wear depth is 20.88 µm. For the average wear volume, the experimental tests resulted in 0.79±0.52 mm^3 while the FE-simulation predicted a maximum of 1.28475 mm^3. The possible cause of the difference between experimental and simulation results may be that the experiment fretting tests were conducted in a chemical environment. Despite this and taking into account the spread in experimental results, the FE-predictions are satisfactory and could investigate the evolution of different variables in the contact zone.

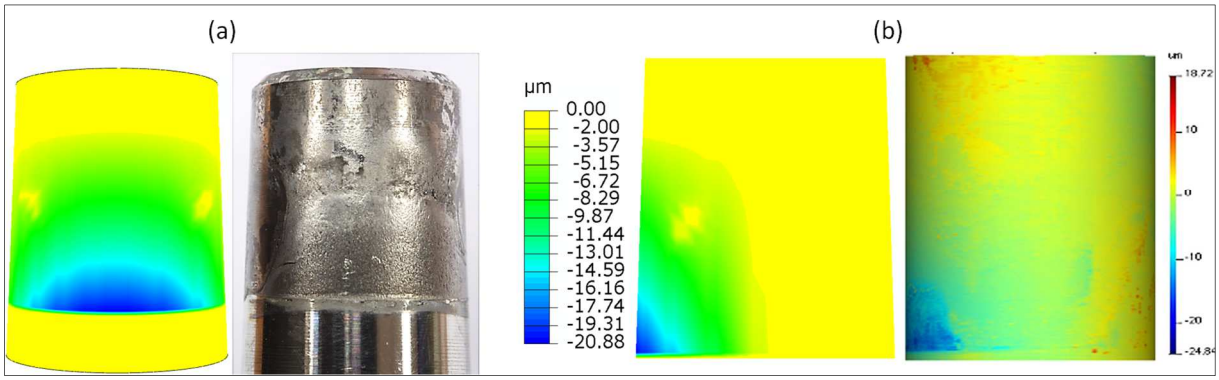

Figure 8. Comparison of FE simulation and experimental results:

(a) FE wear scar (left) vs. experimental wear scar (right) [8]. (b) FE predicted wear depth (left) vs. experimental surface profile: yellow represents the unworn area and the blue the worn surface (right) [35]

3.3. Evolution of fretting wear variables

This section provides the evolution of contact variables over 10 million cyclic loadings obtained by the FE simulation. The cyclic loading applied corresponds to a high peak walking loads of a subject with a bodyweight of 1kN [39; 40]. This is equivalent to about 10 years of operation of moderately intense walking [13].
Figure 9 presents the variation in maximum contact pressure, contact slip, and total wear depth over the taper. Both of inferior and superior sides of the taper are visualized at the different number of cycles.

From **Fig 9a**, it can be seen that the maximum contact pressure is concentrated at the proximal edge of the superior side while keeping an increasing pace over time. On the inferior side, the contact pressure peak is located at the distal, but its position changes towards the middle, after about one million cycles.

For the relative contact slip, the highest values are located above the distal edge of the inferior side and no-slip is induced in the proximal edge of the superior side (**Fig 9b**). This location of the highest contact variables at the two diagonally opposite contact edges is the result of the rocking motion due to the subjected bending load on the hip neck. As the wear is the product of contact pressure and contact slip, the maximum wear depth is found to be mainly concentrated at the distal edge of the taper inferior side (**Fig 9c**) with a maximum of 20.88 µm. On the superior side, a slight amount of wear depth was predicted with a maximum of 2.92 µm and located in the borders of the main wear scar. For the fretting interaction analysis, only the results of the inferior side are considered, as this region is the most critical.

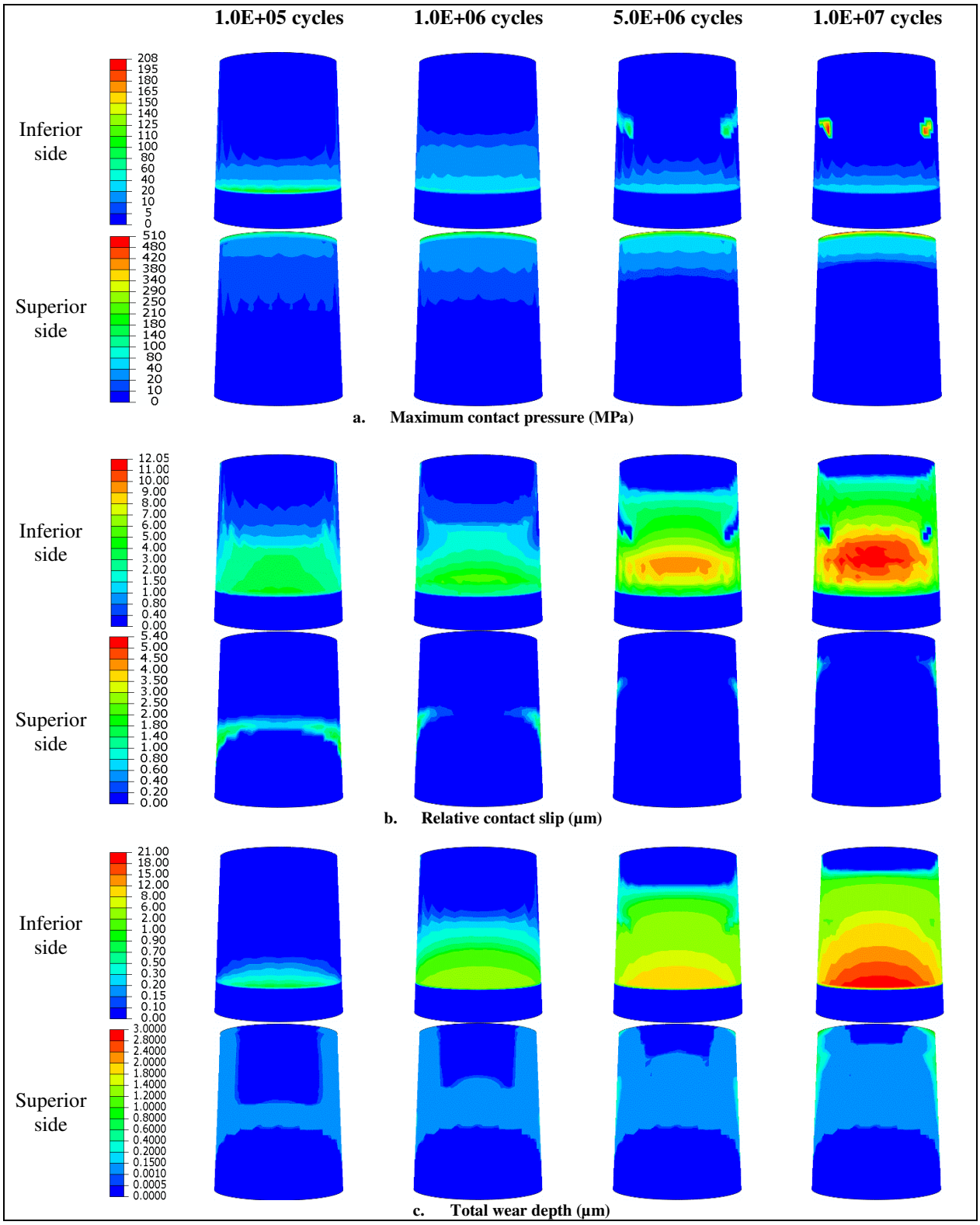

Figure 9. Variation of contact variables on the taper

Figures 10a and **10b** shows the evolution of linear wear depth along the circular and the median profile at a different number of cycles. It can be observed that a little wear scar occurs initially at the middle of the distal

edge. The material removal at this area releases contact between master and slave elements and results in a significant decreasing of the contact pressure, from 95 MPa at 1E+05 cycles to 48 MPa at 1E+06 cycles (**Figs 10c and 10d**). In return, the concomitant relative contact slip remains almost unchanged around 4 to 5 µm before 1E+05 cycles, then increases rapidly to reach a maximum of 12.13 µm at 1E+07 cycles (**Fig 11**). As a consequence of contact variables evolving, the wear scar becomes wider with time and broadens towards the median region of the taper, from 0.25 of the normalized median profile at 1E+05 cycles to 0.9 at 1E+07 cycles (**Fig 10b**). The maximum predicted wear depth in the taper is found to be 20.88 µm. Furthermore, the total volume of material removed due to wear is 1.28475 mm^3, which is equivalent to a rate of 0.128475 mm^3/million load cycles.

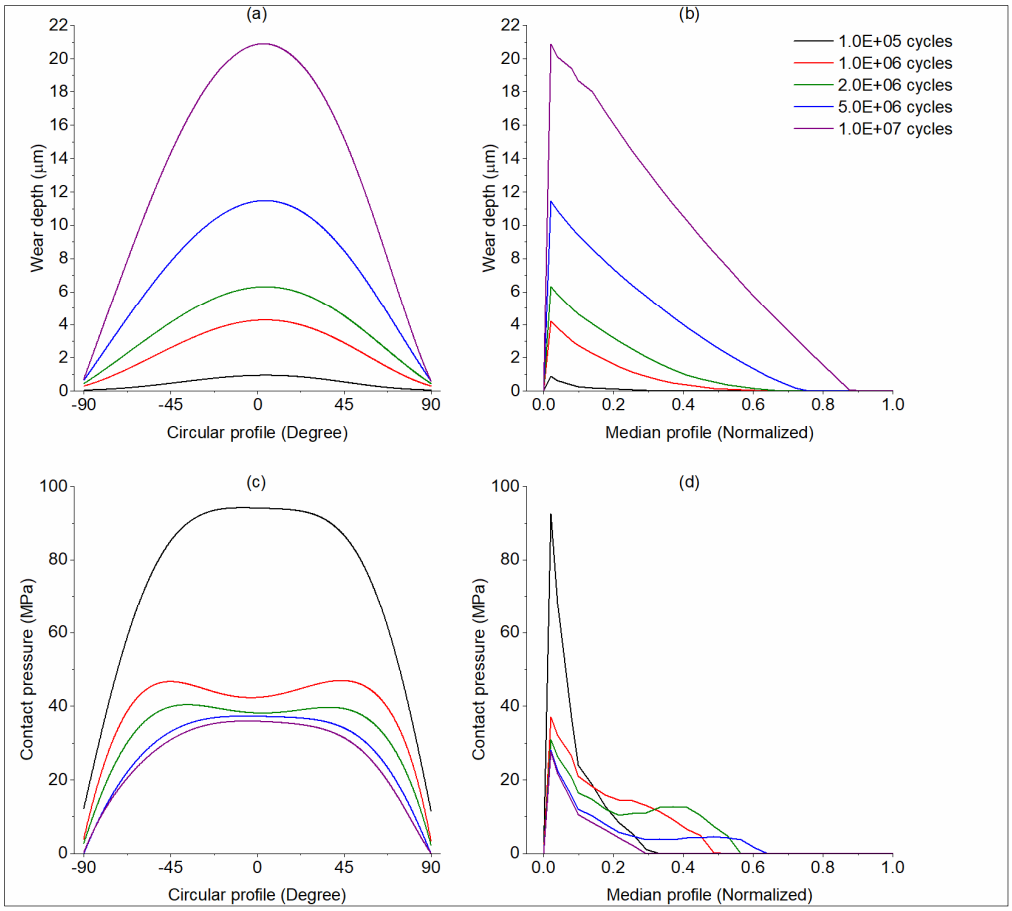

Figure 10. Evolution of: wear depth along: (a) circular profile (b) median profile, contact pressure along: (c) circular profile (d) median profile

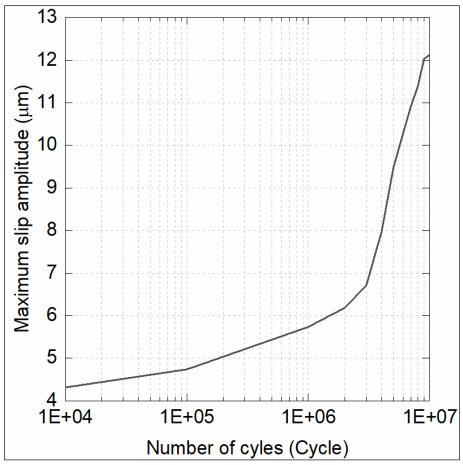

Figure 11. Evolution of the maximum slip amplitude vs the number of cycles

Figure 12a shows the evolution of tribological mechanisms "Stick" and "Slip" in the contact area vs. the number of loading cycles. During the first phase (<10^5 cycles), the stick phenomenon is stable and represents 54%. On the other hand, the slip phenomenon represents 13% with a slight evolution (<5 µm). During this period, fatigue loading is dominant without leading to crack initiation because the maximum stress level represents 30% of the yielding stress (**Fig 12b**). This also means that the material behavior is still elastic and no plastic deformation is occurring. In the second phase (10^5 – 2.10^6 cycles), the proportion of stick drops to the detriment of the slip increase to reach 35% for each contact condition. During this phase, a slight increase in the stress (σ_{11}) is observed. This, is certainly due to the stress concentration at the interface between the stick and slip zones. After 2.10^6 cycles, the slip continues to increase up to 12.13 µm, while the stick drops sharply. This indicates that wear becomes predominant over fatigue.

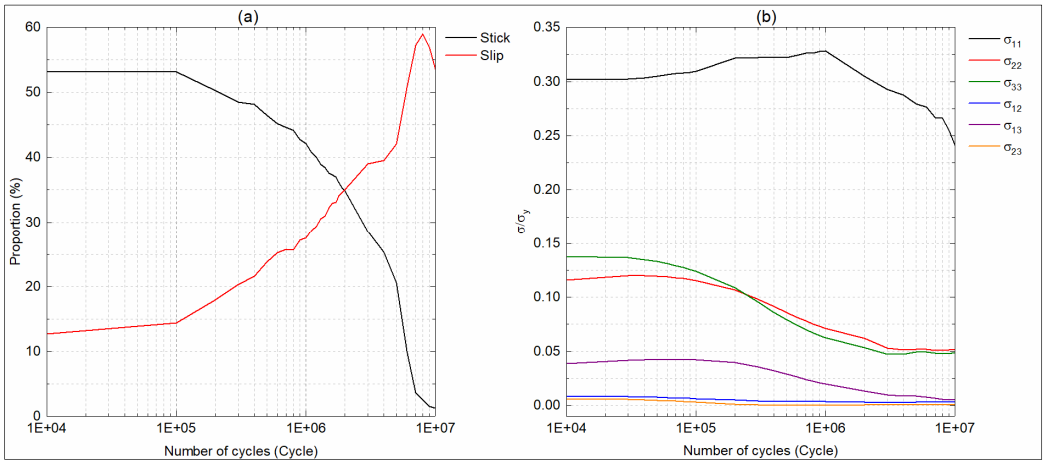

Figure 12. Evolution of: (a) stick and slip proportions (b) stress ratio

3.4. Evolution of fatigue parameters

From the results showing the distribution and the evolution of slip amplitude, three main fretting regions can be identified. A region I where the slip amplitude of their elements varies considerably along cyclic loadings, from about 4 µm to 12.13 µm. This region is mainly located from the distal contact edge to the median area of the inferior side (within the wear scar area). A second region (II) where the slip amplitude of their elements is almost unchanged around 3 µm over time. Such a region is, in particular, situated at the borders of the wear scar. A region III where the contact conditions are non-existent and no wear is induced. This region is located at the distal edge of the superior side of the taper. **Figure 13** shows the evolution of the maximum values of fatigue parameters SWT and FS in regions I, II and III. The highest values of both fatigue parameters are found in the first fretting region. In the first few thousand cycles, the value of SWT parameter increases in a faster way and reaches its maximum (0.7256 MPa) around 1E+05 cycles. Then, it remains constant until up to 1E+06 cycles, and beyond, it starts to decrease progressively to reach a value of 0.53 MPa at the simulation end. At the same time, the SWT parameter takes an upward trend in the second fretting region and remains almost constant in the third fretting region. The lowest predicted fatigue life (corresponding to the highest SWT value) is found to be 1.45E+07 cycles. On the other hand, in the first region, the parameter FS increases up to 0.0036 MPa at 1E+05 cycles and then decreases to reach negligible values near the simulation end. However, for the other regions, FS values are insignificant. The lowest predicted fatigue life (corresponding to the highest FS value) is found to be higher than 3.7E+07 cycles, which is three times greater than the SWT fatigue life. Based on these results, two conclusions may be drawn for the taper investigation. First, the variation over time of fatigue parameters is more significant in the region where wear is predominant. Second, the parameter SWT is more pertinent than the FS parameter; therefore, the stresses-strains induced by the applied forces are mainly tensile-based.

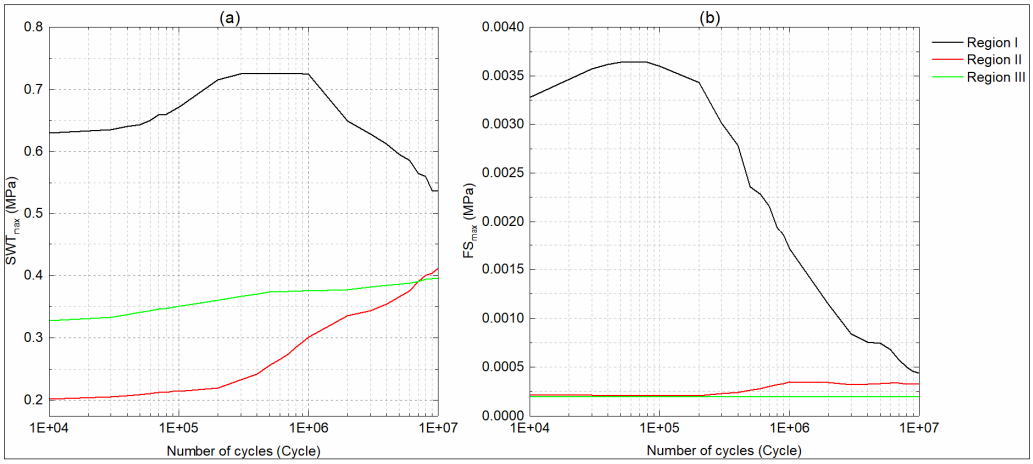

Figure13. Evolution in different fretting zones of: (a) SWT_{max} and (b) FS_{max}

3.5. Effect of fretting wear on the fretting fatigue

Figure 14 depicts the evolution of the accumulated fatigue damage within the first region. The maximum fatigue damage obtained until the end of the simulation is 0.3. This indicates that the distal contact edge of the inferior side presents the most likely site for fatigue crack initiation, although no crack initiation is predicted to appear before 1E+07 cycles. This site is also corresponding to the most worn area in the taper. Furthermore, it can be seen that a significant damage accumulation is observed up to 2E+06 cycles followed by a moderate increase until the end. This reveals that an interaction has occurred along cyclic loading and the fatigue damage accumulation has been affected by the fretting wear regime in this zone. **Figure 15** shows the impact of increasing slip amplitude on the predicted number of cycles to crack initiation. The predicted life is reduced to the minimum (1.7E+07 cycles) under a slip amplitude less than slip 5.75 µm, which corresponds with the stick-slip regime behavior favorable to crack initiation. Once the slip amplitude exceeds this value, the fatigue life increases sharply to almost 7E+07 cycles. This, means that the slip amplitude increasing has led to delay or remove the fatigue crack initiation and therefore enhance the fatigue life. For a better illustration of the dominant damage mechanisms, the concept of "fretting map" was employed to determine the fretting regimes and transition between them. The fretting map is a diagram representing the significant regimes in two variables, with boundaries showing values that correspond to the transition from one regime to another [41]. **Figure 16** is an example of a fretting map reproducing the variation of the volumetric wear rate and fatigue damage rate with changes to the slip amplitude. As can be seen, low slip amplitudes (4.73 ~ 5.75 µm) are associated with the partial slip regime (stick-slip) where high fatigue damage rates and low volumetric wear rates are recorded. The high slip amplitudes (5.75 ~ 12.13 µm) are associated with the gross slip regime where high volumetric wear rates and low fatigue damage rates are obviously shown. The transition from the partial slip to the gross slip regime is produced at a slip amplitude in the vicinity of 5.75 µm. This value is considered as critical for the taper junction as it is experiencing the lowest fatigue life.

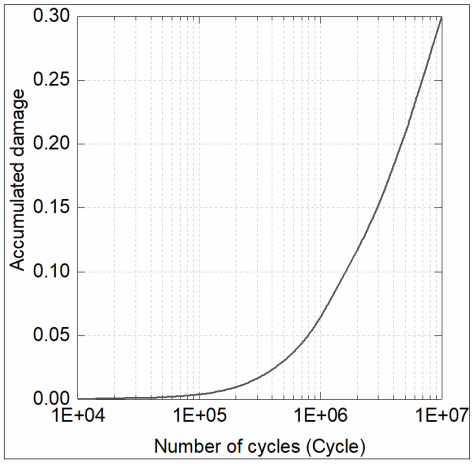

Figure 14. Evolution of the accumulated damage

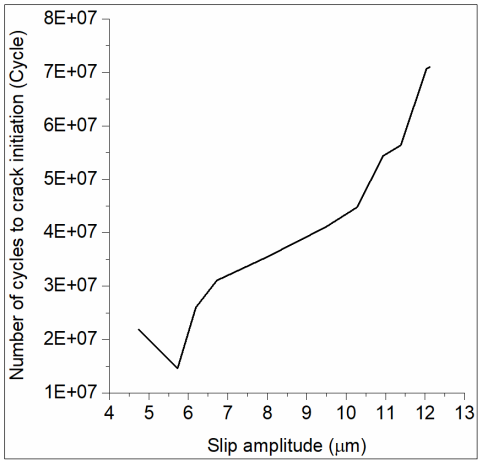

Figure 15. Variation of the number of cycles to crack initiation versus slip amplitude evolution

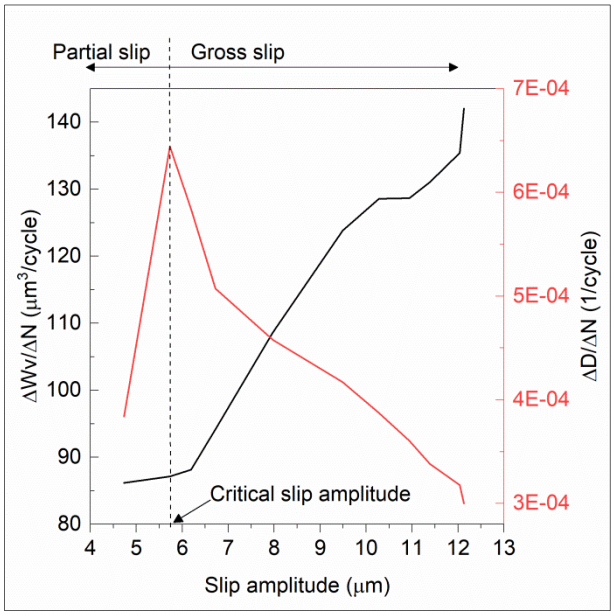

Figure 16. Variation of wear volume rate and fatigue damage rate vs. the slip amplitude

4. Discussion

Fretting wear and fatigue findings obtained using the developed methodology are in agreement with the fretting map concept [41] and experiments conducted on Ti6Al4V specimen (cylinder on-plane) [42][32]. In the literature, the relative contact slip amplitude at the taper junction is considered as a key parameter in the wear process. It was measured under different biomechanical conditions using experimental and computational methods. An average value of the slip amplitude (micro-motion) was found to vary from 3 µm to around 40 µm under different assembly loads and the corresponding volumetric wear rate was from 0.128 mm^3/year to 0.423 mm^3/year [13]. The material combination and corrosion conditions could vary the slip amplitude from 3 µm to 18 µm [10]. In this study, the slip amplitude is found to vary from 4 µm to 12.13 µm and the average volumetric wear rate is around 0.13 mm^3/year.

On the other hand, fatigue tests performed on seven standards (12/14) taper junction revealed that the cracks nucleate in the smallest neck cross-section just below the head [43]. The fatigue failure was found to produce after an average of one million cycles at a maximum load of 6.5 kN. These findings are in full agreement with the obtained results of our performed simulation. The high values of the number of cycles to failure that have been predicted by the simulation can be explained by the fact that only the walking forces (4 kN) were taken into consideration. However, these forces can reach a value of 11kN in case of an obese or very active patient under frequent stumbling [40].

In the present study, the FE prediction of different contact variables and fatigue parameters is based on a 3D model replicating the multidirectional and asymmetrical aspect of the hip implant loads. The induced contact variables and stress distributions are highlighted to be non-symmetrical (**Fig 9**). This results in the localization of both wear scar and crack site in the inferior side of the taper junction, especially around the distal contact edge. In a similar computational investigation, Zhang et al. [23] simulated 5.5 million moderately intense walking in a 2D axisymmetric model of a CoCr/Ti-alloy head-neck taper junction. A maximum wear depth of 1.07 µm was found to be produced at the root of the taper. A very high fatigue life, exceeding 100 million cycles, was predicted based on calculated values of SWT. In another study, Zhang et al. [24] employed the same 2D axisymmetric while including repetitive undulations on a single contact segment. Accordingly, the linear wear depth was estimated to reach a maximum of 7.56 µm i.e. seven times greater than those obtained in the first investigation. The fatigue life was predicted to be 89 million cycles while considering the wear effect. The authors concluded that the effect of the surface undulations on the fatigue life is negligible. The use of a 2D axisymmetric model simplifies the hip implant loading and leads to inconsistencies when compared to available experimental results. This reinforces the argument that 3D models should be used for the simulation of mechanical behavior in THP [25].

The computational methodology developed in this paper has been shown to produce satisfactory results whether for fatigue or wear. Moreover, it has revealed that wear and fatigue mechanisms interact at the surface of the taper depending on the slip amplitude. This is in full agreement with the literature, where the effect of the slip amplitude was found to be critical for both fretting wear and fatigue [19], [32; 33]. Herein, the wear volume is shown to be increased at high slip amplitudes and to be minimal during the partial slip regime. Designers' concern to reduce wear by reducing slip amplitude in the taper junction should not be at the expense of fretting fatigue failure risks. In this study, the fatigue life is found to be significantly decreased at a critical slip amplitude. The change from this critical value is also shown to considerably affect the fatigue life. Furthermore, the variation of the fatigue damage rate is revealed to be abrupt compared to the volumetric wear rate which is typically more progressive and gradual (see **Fig 16**). This makes the fatigue failure even more dangerous for the taper junction. For these reasons, a compromise between wear and fatigue must be established to minimize prosthesis failure and improve their longevity. The presented methodology may be used in future work in combination with more advanced optimization techniques to minimize both fatigue damage and volumetric wear. On this basis, the optimal design leading to operating the prosthesis in an appropriate range of slip amplitude can be also determined. The FE prediction of contact variables over a high number of loading cycle permits to identify the critical value of the slip amplitude in which the fatigue life is minimum. For the operational conditions of the hip implant considered in this study, a critical value of 5.75 µm is determined.

Although the developed methodology was able to model both fretting wear, fatigue and interaction between them, there are possible shortcomings and limitations. In the literature, it is recognized that fretting wear, corrosion and their interactions play an important role in predicting the life cycle of THR. However, in the present study, the estimation of wear was performed based solely on the mechanical fretting wear according to the Archard law. This was adopted as the fretting wear is considered as the primary mechanism causing surface damage, and should precede chemical alteration [12]. In fact, it is important to keep in mind that the taper junction is continuously subjected to mechanically assisted corrosion which may accelerate the degradation even in the absence of the load [15]. Hence, it is evident that further developments are required to enhance the prediction quality by considering the effect of fretting corrosion. On the other hand, the effect of the material removal on the mechanical behavior and resulting fatigue life was considered by employing the adaptive meshing technique. However, cyclic fatigue hardening may also affect the stress/strain distribution and leads to the shortening of the fatigue life. In the actual investigation, very low-stress values were revealed to be induced at the taper junction, and no plastic deformation was produced (see **Fig 12b**). Accordingly, the effect of cyclic hardening was not considered in this study.

5. Conclusion

This study deals with a combined 3D FE-based methodology to understand and predict fretting fatigue and wear behavior in a taper junction of a modular hip prosthesis. A computational time optimization and a validation against available experimental data have been carried out. The performed simulation has allowed investigating the contact variables evolution, the wear-induce fatigue parameters, and consequently more understanding of the fretting mechanisms. The effect of fretting wear on the fatigue life and crack initiation site has been commented. Based on our findings, the main conclusions are:

- During the operating life of a prosthesis, the taper junction is going through a partial slip regime where the risks of failure by fatigue damage are very high. This phase is followed by a transition to a gross slip regime where a high wear rate is recorded.
- Fretting regime transition is mainly controlled by the contact slip amplitude, and consequently the contact pressure and stress concentration.
- The determination of the critical slip amplitude, in which the fatigue life is minimum, is important to operate the prostheses in a safety zone. This is an essential key which contributes to the development of novel taper designs.
- Finally, the use of the developed methodology to study the influence of different design parameters, clinical aspects and tribological concerns on the fretting behavior in taper junctions will be a logical sequel to this work.

References

[1] T. M. Grupp, T. Weik, W. Bloemer, and H.-P. Knaebel, "Modular titanium alloy neck adapter failures in hip replacement - failure mode analysis and influence of implant material," BMC Musculoskelet. Disord., vol. 11, no. 1, p. 3, Dec. 2010, doi: 10.1186/1471-2474-11-3.

[2] C. R. Nahhas, P. H. Yi, M. Moric, R. Puri, J. J. Jacobs, and S. M. Sporer, "High Failure at a Minimum 5-Year Follow-Up in Primary Total Hip Arthroplasty Using a Modular Femoral Trunnion," J. Arthroplasty, vol. 34, no. 7, pp. 1395–1399, Jul. 2019, doi: 10.1016/j.arth.2019.03.033.

[3] S. K. Fokter, V. Levašič, and S. Kovač, "The innovation trap: Modular neck in total hip arthroplasty," Zdr. Vestn., vol. 86, no. 3–4, pp. 115–126, 2017.

[4] K. Osman, A. P. Panagiotidou, M. Khan, G. Blunn, and F. S. Haddad, "Corrosion at the head-neck interface of current designs of modular femoral components," Bone Joint J., vol. 98-B, no. 5, pp. 579–584, May 2016, doi: 10.1302/0301-620X.98B5.35592.

[5] Z. H. Goldstein, K. Estrera, and B. R. Levine, "Taper Failure After Large-Diameter Metal-on-Metal Total Hip Arthroplasty," Orthopedics, vol. 39, no. 5, pp. e984–e987, Sep. 2016, doi: 10.3928/01477447-20160526-07.

[6] G. Ullmark, "Femoral Head Fractures: Hemiarthroplasty or Total Hip Arthroplasty?," HIP Int., vol. 24, no. 10_suppl, pp. 12–14, Jun. 2014, doi: 10.5301/hipint.5000167.

[7] J. J. Williams and N. Chawla, "Fractography of a neck failure in a double-modular hip implant," Case Stud. Eng. Fail. Anal., vol. 2, no. 1, pp. 45–50, Apr. 2014, doi: 10.1016/j.csefa.2014.03.001.

[8] T. Bitter, I. Khan, T. Marriott, E. Lovelady, N. Verdonschot, and D. Janssen, "A combined experimental and finite element approach to analyse the fretting mechanism of the head–stem taper junction in total hip replacement," Proc. Inst. Mech. Eng. Part H J. Eng. Med., vol. 231, no. 9, pp. 862–870, Sep. 2017, doi: 10.1177/0954411917713774.

[9] C. T. dos Santos, C. Barbosa, M. J. Monteiro, I. C. Abud, I. M. V. Caminha, and C. R. M. Roesler, "Characterization of the fretting corrosion behavior, surface and debris from head-taper interface of two different modular hip prostheses," J. Mech. Behav. Biomed. Mater., vol. 62, pp. 71–82, Sep. 2016, doi: 10.1016/j.jmbbm.2016.04.036.

[10] S. Y. Jauch, G. Huber, E. Hoenig, M. Baxmann, T. M. Grupp, and M. M. Morlock, "Influence of material coupling and assembly condition on the magnitude of micromotion at the stem–neck interface of a modular hip endoprosthesis," J. Biomech., vol. 44, no. 9, pp. 1747–1751, Jun. 2011, doi: 10.1016/j.jbiomech.2011.04.007.

[11] H. Haschke, S. Y. Jauch-Matt, K. Sellenschloh, G. Huber, and M. M. Morlock, "Assembly force and taper angle difference influence the relative motion at the stem–neck interface of bi-modular hip prostheses," Proc. Inst. Mech. Eng. Part H J. Eng. Med., vol. 230, no. 7, pp. 690–699, Jul. 2016, doi: 10.1177/0954411916648717.

[12] R. English, A. Ashkanfar, and G. Rothwell, "A computational approach to fretting wear prediction at the head–stem taper junction of total hip replacements," Wear, vol. 338–339, pp. 210–220, Sep. 2015, doi: 10.1016/j.wear.2015.06.016.

[13] R. English, A. Ashkanfar, and G. Rothwell, "The effect of different assembly loads on taper junction fretting wear in total hip replacements," Tribol. Int., vol. 95, pp. 199–210, Mar. 2016, doi:

10.1016/j.triboint.2015.11.025.

[14] K. Fallahnezhad, R. H. Oskouei, H. Badnava, and M. Taylor, “An adaptive finite element simulation of fretting wear damage at the head-neck taper junction of total hip replacement: The role of taper angle mismatch,” J. Mech. Behav. Biomed. Mater., vol. 75, pp. 58–67, Nov. 2017, doi: 10.1016/j.jmbbm.2017.07.003.

[15] K. Fallahnezhad, R. H. Oskouei, and M. Taylor, “Development of a fretting corrosion model for metallic interfaces using adaptive finite element analysis,” Finite Elem. Anal. Des., vol. 148, pp. 38–47, Sep. 2018, doi: 10.1016/j.finel.2018.05.004.

[16] A. Ashkanfar, D. J. Langton, and T. J. Joyce, “A large taper mismatch is one of the key factors behind high wear rates and failure at the taper junction of total hip replacements: A finite element wear analysis,” J. Mech. Behav. Biomed. Mater., vol. 69, no. November 2016, pp. 257–266, May 2017, doi: 10.1016/j.jmbbm.2017.01.018.

[17] H. C. Lee, Y. Lee, S. Y. Lee, S. Choi, D. L. Lee, and Y. T. Im, “Tool life prediction for the bolt forming process based on high-cycle fatigue and wear,” J. Mater. Process. Technol., vol. 201, no. 1–3, pp. 348–353, May 2008, doi: 10.1016/j.jmatprotec.2007.11.166.

[18] J. Ding, S. B. Leen, E. J. Williams, and P. H. Shipway, “Finite element simulation of fretting wear-fatigue interaction in spline couplings,” Tribol. - Mater. Surfaces Interfaces, vol. 2, no. 1, pp. 10–24, Mar. 2008, doi: 10.1179/175158308X320791.

[19] A. Cruzado, S. B. Leen, M. A. Urchegui, and X. Gómez, “Finite element simulation of fretting wear and fatigue in thin steel wires,” Int. J. Fatigue, vol. 55, pp. 7–21, Oct. 2013, doi: 10.1016/j.ijfatigue.2013.04.025.

[20] S. M. O’Halloran, P. H. Shipway, A. D. Connaire, S. B. Leen, and A. M. Harte, “A combined wear-fatigue design methodology for fretting in the pressure armour layer of flexible marine risers,” Tribol. Int., vol. 108, no. October 2016, pp. 7–15, Apr. 2017, doi: 10.1016/j.triboint.2016.10.020.

[21] Y. B. Zhang, L. T. Lu, L. Zou, D. F. Zeng, and J. W. Zhang, “Finite element simulation of the influence of fretting wear on fretting crack initiation in press-fitted shaft under rotating bending,” Wear, vol. 400–401, no. January, pp. 177–183, Apr. 2018, doi: 10.1016/j.wear.2018.01.008.

[22] M. Baxmann, S. Y. Jauch, C. Schilling, W. Blömer, T. M. Grupp, and M. M. Morlock, “The influence of contact conditions and micromotions on the fretting behavior of modular titanium alloy taper connections,” Med. Eng. Phys., vol. 35, no. 5, pp. 676–683, May 2013, doi: 10.1016/j.medengphy.2012.07.013.

[23] T. Zhang, N. M. Harrison, P. F. McDonnell, P. E. McHugh, and S. B. Leen, “A finite element methodology for wear–fatigue analysis for modular hip implants,” Tribol. Int., vol. 65, pp. 113–127, Sep. 2013, doi: 10.1016/j.triboint.2013.02.016.

[24] T. Zhang, N. M. Harrison, P. F. McDonnell, P. E. McHugh, and S. B. Leen, “Micro–macro wear–fatigue of modular hip implant taper-lock coupling,” J. Strain Anal. Eng. Des., vol. 49, no. 1, pp. 2–18, Jan. 2014, doi: 10.1177/0309324713502175.

[25] G. Bergmann, A. Bender, J. Dymke, G. Duda, and P. Damm, “Standardized Loads Acting in Hip Implants,” PLoS One, vol. 11, no. 5, p. e0155612, May 2016, doi: 10.1371/journal.pone.0155612.

[26] I. . McColl, J. Ding, and S. . Leen, “Finite element simulation and experimental validation of fretting wear,” Wear, vol. 256, no. 11–12, pp. 1114–1127, Jun. 2004, doi: 10.1016/j.wear.2003.07.001.

[27] S. Fouvry, T. Liskiewicz, and C. Paulin, “A global–local wear approach to quantify the contact endurance under reciprocating-fretting sliding conditions,” Wear, vol. 263, no. 1–6, pp. 518–531, Sep. 2007, doi: 10.1016/j.wear.2007.01.072.

[28] Dassault, “ABAQUS Documentation,” ABAQUS/CAE Doc., pp. 1–847, 2016.

[29] A. Belloula, A. Amrouche, M. Nait-Abdelaziz, and N. Benseddiq, “Comparison of the cracking energy density and the Smith-Watson-Topper parameters in predicting fretting fatigue lifetime of a steel/aluminum alloy contact,” Fatigue Fract. Eng. Mater. Struct., vol. 37, no. 12, pp. 1355–1366, Dec. 2014, doi: 10.1111/ffe.12252.

[30] J. Araújo, “The effect of rapidly varying contact stress fields on fretting fatigue,” Int. J. Fatigue, vol. 24, no. 7, pp. 763–775, Jul. 2002, doi: 10.1016/S0142-1123(01)00191-8.

[31] W. SUM, E. WILLIAMS, and S. LEEN, “Finite element, critical-plane, fatigue life prediction of simple and complex contact configurations,” Int. J. Fatigue, vol. 27, no. 4, pp. 403–416, Apr. 2005, doi: 10.1016/j.ijfatigue.2004.08.001.

[32] J. J. Madge, S. B. Leen, and P. H. Shipway, “The critical role of fretting wear in the analysis of fretting fatigue,” Wear, vol. 263, no. 1–6, pp. 542–551, Sep. 2007, doi: 10.1016/j.wear.2006.11.021.

[33] J. J. Madge, S. B. Leen, I. R. McColl, and P. H. Shipway, “Contact-evolution based prediction of fretting fatigue life: Effect of slip amplitude,” Wear, vol. 262, no. 9–10, pp. 1159–1170, Apr. 2007, doi: 10.1016/j.wear.2006.11.004.

[34] T. Bitter, I. Khan, T. Marriott, B. W. Schreurs, N. Verdonschot, and D. Janssen, “Experimental Measurement of the Static Coefficient of Friction at the Ti–Ti Taper Connection in Total Hip Arthroplasty,” J. Biomech. Eng., vol. 138, no. 3, Mar. 2016, doi: 10.1115/1.4032446.

[35] T. Bitter, I. Khan, T. Marriott, E. Lovelady, N. Verdonschot, and D. Janssen, “Finite element wear prediction using adaptive meshing at the modular taper interface of hip implants,” J. Mech. Behav. Biomed. Mater., vol. 77, no. May 2017, pp. 616–623, Jan. 2018, doi: 10.1016/j.jmbbm.2017.10.032.

[36] A. Cruzado, M. A. Urchegui, and X. Gómez, “Finite element modeling and experimental validation of fretting wear scars in thin steel wires,” Wear, vol. 289, pp. 26–38, Jun. 2012, doi: 10.1016/j.wear.2012.04.018.

[37] Y. Zhang, L. Lu, Y. Gong, J. Zhang, and D. Zeng, “Finite Element Modeling and Experimental Validation of Fretting Wear Scars in a Press-Fitted Shaft with an Open Zone,” Tribol. Trans., vol. 61, no. 4, pp. 585–595, Jul. 2018, doi: 10.1080/10402004.2017.1378395.

[38] K. Pereira et al., “On the Convergence of Stresses in Fretting Fatigue,” Materials (Basel)., vol. 9, no. 8, p. 639, Jul. 2016, doi: 10.3390/ma9080639.

[39] G. Bergmann, F. Graichen, and A. Rohlmann, “Hip joint loading during walking and running, measured in two patients,” J. Biomech., vol. 26, no. 8, pp. 969–990, Aug. 1993, doi: 10.1016/0021-9290(93)90058-M.

[40] G. Bergmann et al., “Realistic loads for testing hip implants,” Biomed. Mater. Eng., vol. 20, no. 2, pp. 65–75, 2010, doi: 10.3233/BME-2010-0616.

[41] O. Vingsbo and S. Söderberg, “On fretting maps,” Wear, vol. 126, no. 2, pp. 131–147, Sep. 1988, doi: 10.1016/0043-1648(88)90134-2.

[42] O. Jin and S. Mall, “Effects of slip on fretting behavior: experiments and analyses,” Wear, vol. 256, no. 7–8, pp. 671–684, Apr. 2004, doi: 10.1016/S0043-1648(03)00510-6.

[43] M. Nganbe, H. Louati, U. Khan, A. Speirs, and P. E. Beaulé, “Retrieval analysis and in vitro assessment of strength, durability, and distraction of a modular total hip replacement,” J. Biomed. Mater. Res. Part A, vol. 95A, no. 3, pp. 819–827, Dec. 2010, doi: 10.1002/jbm.a.32886.